Microcavity polariton spin quantum beats without a magnetic field: A manifestation of Coulomb exchange in dense and polarized polariton systems

P. Renucci, T. Amand, and X. Marie
Laboratoire de Nanophysique, Magnétisme et Optoélectronique—LNMO/INSA, INSA, 135 avenue de Rangueil, F-31077 Toulouse Cedex 4, France

P. Senellart, J. Bloch, and B. Sermage
Laboratoire de Photonique et Nanostructures, Route de Nozay 91460 Marcoussis, France

K. V. Kavokin
A. F. Ioffe Physico-Technical Institute, Polytechnicheskaya, 26, St. Petersburg 194021, Russia
(Received 9 September 2004; revised manuscript received 14 April 2005; published 5 August 2005)

Microcavity polariton spin dynamics is investigated in high-finesse microcavities under resonant excitation using polarization- and time-resolved secondary emission spectroscopy. Using an appropriate calibration procedure, the instantaneous polariton occupation numbers of the modes with $\mathbf{k}\approx\mathbf{0}$ wave vectors can be determined. When the phase-matching conditions are achieved, we show that Coulomb scattering dominates the other processes, and that stimulation occurs when the occupation of the $\mathbf{k}\approx\mathbf{0}$ final state with a given mode polarization approaches unity. Under elliptically polarized light, we show that the stimulated polariton scattering leads to an increase with time of the circular polarization of the $\mathbf{k}\approx\mathbf{0}$ states, while the linear polarization dynamics is characterized first by a fast drop to negative or zero values immediately after the excitation pulse, followed by weak-amplitude nonperiodic oscillations. The latter are interpreted as the manifestation of the pseudospin precession of the pumped polariton modes around the self-induced exchange effective field.

DOI: 10.1103/PhysRevB.72.075317 PACS number(s): 78.47.+p, 42.50.Md, 71.35.Lk, 71.36.+c

I. INTRODUCTION

Semiconductor microcavities have attracted strong interest since the demonstration of strong coupling.[1] More recently, this interest was renewed by the discovery of resonant parametric scattering of exciton-polariton pairs.[2–7] This effect has some analogies with optical parametric processes such as four-wave mixing in nonlinear optical crystals,[7–9] although matter waves are involved here instead of crystal photon modes. Various effects such as huge amplification in pump-probe experiments,[2,4,6] blueshift of the polariton modes,[2,4,6,9] and parametric luminescence[3,5] are well accounted for within this approach. The polaritons are treated here as a weakly interacting boson system, the interaction being essentially driven by Coulomb exchange. When the uncoupled photon mode E_C is located below or close to the exciton one E_X (i.e., at negative or zero detuning δ, $\delta = E_C - E_X$), the polariton branches present high energy dispersion, a consequence of the photon component of this mixed exciton-photon quasiparticle.[1] As a consequence, high occupancy numbers without significant phase-space filling can be reached, thus paving the way for achieving Bose condensates. The observed deamplification down to the shot noise in degenerate polariton four-wave mixing opens the way to squeezing in semiconductor microcavity devices.[9]

However, despite the renewed interest in spin properties with the advent of *spintronics*, i.e., the possibility to design devices in which spin-dependent functions are achieved (see, e.g., Ref. 10), the spin properties of high-finesse microcavities have been considered only recently. Drastic changes with respect to the bare exciton case are expected due to the photon component of the polaritons. In pump-probe experiments, the polariton spin properties manifest as polarization selections rules for the probe with respect to the pump; early works show that, using circularly polarized light, giant amplification occurs only if the pump and the probe are cocircularly polarized,[2,11,12] while more subtle selection rules occur in the case of a linear pump and circular probe.[12] In luminescence experiments, early works on polariton spin dynamics were performed in the spontaneous emission regime; for instance, the polariton spin relaxation is quenched at negative detuning.[13] Polariton spin or alignment manipulations by temporal coherent control experiments could even be achieved.[14] Under stimulated regime, a complex polarization behavior of the emission is observed, depending both on the excitation spectral energy and density power; in pulsed experiments, a sign reversal of the lower-branch (LB) circular polarization with respect to the pump has been even observed at negative cavity detuning when exciting above the quantum-well light-hole exciton transition with circularly polarized light, with increased marked effect when the excitation power is raised; at positive detuning the effect is the opposite on the upper branch (UB).[15] Under cw resonant LB excitation, the LB emission polarization and intensity dependence on the excitation ellipticity has been explored, showing a nonmonotonic behavior of the LB circular polarization rate, with an optimum for both at a circular polarization degree of about 0.5.[8]

Here we address polariton spin dynamics through time-resolved spectroscopy of the microcavity secondary emission under resonant pumping of the LB, under the conditions of dominant Coulomb scattering. The aim of this work is to

investigate the consequences of the exchange interaction Hamiltonian on the spin dynamics, through experiments performed under circular or elliptical excitation. The emission polarization behavior is shown to strongly differ from that of resonantly excited dense exciton system,[16] due to the photon character of polaritons. The partial loss of spin coherence between the two polariton spin populations after exchange scattering leads essentially here to an increase of the emission circular polarization degree. However, the linear polarization of the emission displays an unexpected oscillating behavior of limited amplitude. Under strictly linearly polarized excitation, no oscillations are observed, but the linear polarization of the emission is opposite to the pump one. The latter properties are discussed in relation to the Coulomb exchange interaction. The paper is organized as follows. In Sec. II, we present the microcavity samples and the experimental methodology; Sec. III is devoted to the experimental results of time- and polarization-resolved secondary emission, under optical excitation pulses with various ellipticity. In Sec. IV, we discuss the interpretation of the results in the frame of the pseudospin formalism, and propose a possible effective interaction Hamiltonian for spin-polarized dense polariton systems. We finally conclude in Sec. V.

II. MICROCAVITY SAMPLES AND EXPERIMENTAL METHODOLOGY

The experiments were performed on several λ microcavities. We present here the results obtained on the highest-finesse one, characterized by a photon lifetime $\tau_c \sim 8$ ps. It consists of two Bragg mirrors made of 22 (26) $AlAs/Al_{0.1}Ga_{0.9}As$ layers; a single 8-nm-wide $Ga_{0.95}In_{0.05}As$ quantum well is embedded in the middle. The vacuum Rabi splitting is $\Omega_R \approx 3.5$ meV. The cavity is wedged, so that the detuning δ between the cavity and exciton modes could be varied by moving the excitation spot on the sample surface.

The excitation beam, resonant with the polariton LB, is incident at an angle of 8° (±1°), so that it generates LB polaritons in a state with initial in-plane wave vector $k_p = (1 \pm 0.12) \times 10^4$ cm^{-1} [see inset in Fig. 1(c)] along an axis labeled hereafter as Ox. The excitation power density is denoted P_{in}, and the excitation spot diameter is about 100 μm. Its spectral width is about 2 meV. The ellipticity of the incident light is tuned using a Soleil-Babinet compensator. The produced laser pulse with polarization σ^α generates polaritons in the coherent superposition denoted as $|\mathbf{k}_p, \alpha\rangle = \cos\alpha |\mathbf{k}_p, +1\rangle + \sin\alpha |\mathbf{k}_p, -1\rangle$, where $|\mathbf{k}_p, \pm 1\rangle$ represent the polariton states with k_p wave vector and total angular momentum projection $J_z = \pm 1$. The circular (linear) polarization degree of the initially generated polaritons is thus $P_{\text{circ},\mathbf{k}_p} = \cos 2\alpha$ ($P_{\text{lin},\mathbf{k}_p} = \sin 2\alpha$).

The polariton emission is recorded at 10 K using a two-color up-conversion spectroscopy setup, which provides time and spectral resolutions of about 1.5 ps and 2 meV, respectively.[14] In particular, the cavity photon lifetime is deduced from time-resolved emission measurements performed at strong negative cavity detuning ($\delta = -9$ meV). We have characterized experimentally the detection solid angle determined by the frequency-mixing process: it consists in an elliptical cone, normal to the microcavity surface, with aperture half angles $\theta_x \approx 3.8°$ and $\theta_y \approx 0.95°$ in the horizontal (containing Ox) and vertical planes (orthogonal to Ox), respectively. The resulting small acceptance solid angle $\delta\Omega$ ($\delta\Omega \approx 3 \times 10^{-3}$ sr) allows us to detect the polariton modes in the vicinity of $\mathbf{k} \approx \mathbf{0}$.

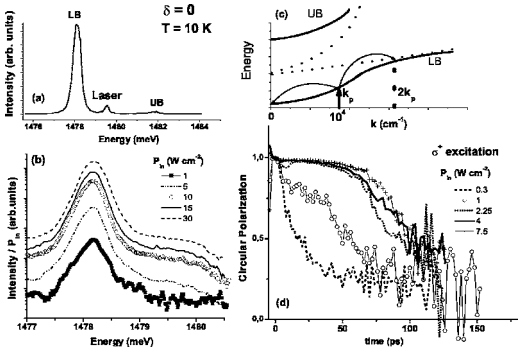

FIG. 1. Microcavity emission spectra at a cavity detuning $\delta = 0$ and resonant excitation with the lower polariton branch. The temperature is 10 K. (a) Cavity emission under a cw excitation of 5 W cm^{-2}, displaying the lower-branch emission. A weak component appears also at higher energy, corresponding to the upper-branch emission. The laser light scattered by the sample surface is also visible. (b) Time-integrated and normalized photoluminescence spectra under resonant linearly polarized pulsed excitation ($\mathbf{k}_p \approx 10^4$ cm^{-1}) for increasing excitation intensities. The arrow indicates the uncoupled cavity photon mode. (c) Polariton dispersion curves in the strong-coupling scheme. The solid lines denote by UB (LB) the upper (lower) branch. Dashed lines: uncoupled exciton and cavity photon modes. The vertical arrow indicates the generated polariton mode. (d) Temporal evolution of the circular polarization degree of the polariton emission under circularly polarized excitation σ^+ for increasing excitation intensities.

In order to determine the dynamics of polariton state occupancy at small wave vectors, we have calibrated our detection setup using a sensitive power meter. It was thus possible to evaluate the number of emitted photons per second $I^\alpha = (dn_{\sigma^\alpha}/dt)(t)$ with a given polarization σ^α in the detection cone. It is related to the polariton occupation number near $k = 0$, denoted $N_{\alpha,k=0}(t)$, by the expression[17,18] $(dn_{\sigma^\alpha}/dt)(t) \approx \frac{1}{2}(A/\lambda_0^2 \tau_0)\delta\Omega N_{\alpha,k=0}(t)$, where A is the excitation spot area, λ_0 is the emission wavelength, and τ_0 is the polariton escape time $\tau_{\mathbf{k}}$ for $\mathbf{k} = 0$ LB polaritons. The factor 1/2 accounts for the fact that the cavity emission is detected from one side only (the top Bragg mirror and the ensemble composed by the back Bragg mirror and the substrate have equivalent reflectivity). The experimentally deduced $N_{\alpha,k=0}(t)$ represents, at low excitation power, the occupancy factor of the polariton modes $|\mathbf{k}_p, \alpha\rangle$ averaged on the small detection cone $\delta\Omega$. We denote the specific occupation numbers $N_{+1(-1),\mathbf{k}}(t) \equiv N_{0(\pi/2),\mathbf{k}}(t)$ as corresponding to $|\mathbf{k}, \pm 1\rangle$ ($\alpha = 0$ and $\pi/2$, respectively) and $N_{x(y),\mathbf{k}}(t) \equiv N_{\pi/4(-\pi/4),\mathbf{k}}(t)$ ($\alpha = \pi/4$ and $-\pi/4$, respectively) to $|\mathbf{k}, X\rangle \equiv |\mathbf{k}, +\pi/4\rangle$ ($|\mathbf{k}, Y\rangle \equiv |\mathbf{k}, -\pi/4\rangle$) state populations at time delay t. In the general case, it is more convenient to work in the polariton density operator formalism $\hat{\rho}_{\mathbf{k}}(t)$, defined by the equation $\hat{\rho}_{\mathbf{k}} = (N_{\mathbf{k}}/2)\hat{I} + \mathbf{S}_{\mathbf{k}} \cdot \hat{\sigma}$. Here, $N_{\mathbf{k}}$ represents the total polariton population and $\mathbf{S}_{\mathbf{k}}$ is the

polariton pseudospin density with wave vector $\mathbf{k}$, $\hat{I}$ is the identity matrix, and $\hat{\sigma}$ is the vector operator built with Pauli matrices.[19] Choosing the states $\{|\mathbf{k},\pm1\rangle\}$ as the basis for wave-vector $\mathbf{k}$ polaritons, the experimentally determined numbers $N_{\pm1,\mathbf{k}}$ correspond in fact to $\hat{\rho}_{\mathbf{k}}$ population terms, and $N_{x(y),\mathbf{k}}$ give access to the real part of the coherence term via the respective relations $N_{\pm1,\mathbf{k}}=(\hat{\rho}_{\mathbf{k}})_{\pm1,\pm1}$ and $N_{x(y),\mathbf{k}}=N_{\mathbf{k}}/2\,{}^{+}_{(-)}\mathrm{Re}\{(\hat{\rho}_{\mathbf{k}})_{-1,+1}\}$. The circular polarization degree of the emission is defined as $P_{\mathrm{circ}}=(I^+-I^-)/(I^++I^-)$, where I^+ (I^-) denote, respectively, the right (left) circularly polarized emission components. The linear polarization along two orthogonal axes is defined as P_{lin} $(P'_{\mathrm{lin}})=(I^{x(x')}-I^{y(y')})/(I^{x(x')}+I^{y(y')})$, where $I^{x(x')}$ and $I^{y(y')}$ denote the linear polarization components along the $\{(1,1,0),(1,\bar{1},0)\}$ [respectively{(1,0,0), (0,1,0)}] crystallographic axes. Using the pseudospin notation, these polarization degrees are simply related to the pseudospin $\mathbf{S}_{\mathbf{k}}$ and population $N_{\mathbf{k}}$ by the relations $P_{\mathrm{lin}}=2(\mathbf{S}_{\mathbf{k}})_x/N_{\mathbf{k}}$, $P'_{\mathrm{lin}}=2(\mathbf{S}_{\mathbf{k}})_y/N_{\mathbf{k}}$, and $P_{\mathrm{circ}}=2(\mathbf{S}_{\mathbf{k}})_z/N_{\mathbf{k}}$. We use similar definitions for the excitation pulse. Note that as we do not measure the diagonal polarization P'_{lin} with our setup, we can only give some upper bound for it.

III. POLARITON SPIN DYNAMICS: EXPERIMENTAL RESULTS

We first recall the circular polarization dynamics under right-hand (σ^+) circularly polarized excitation, at $\delta=0$. Under low excitation power, the polariton circular polarization decreases with a typical time of $T_{s1}\approx30$ ps [see Fig. 1(d)]. We attribute this decay to the splitting between longitudinal and transverse polariton modes in the microcavity.[20,21] However, above a threshold of about $P_{\mathrm{th}}\sim1$ W cm^{-2}, the circular polarization degree decay becomes slower. At the highest investigated excitation power $P_{\mathrm{in}}\approx7.5$ W cm^{-2}, P_{circ} saturates at a value of about 100%, with a plateau which lasts up to 50 ps. We have previously checked carefully that the cavity is in the strong-coupling regime for $P_{\mathrm{in}}\lesssim30$ W cm^{-2}. One can see [Figs. 1(a) and 1(b)] in spectra recorded with a Hamamatsu Streak camera (the spectral resolution of the whole photoluminescence setup is 0.4 meV) that the lower polariton branch lies 1.7 meV below the uncoupled photon mode in this range of excitation power.

In order to describe more accurately the polariton dynamics within the lower branch, we have extracted the polariton state occupancy at small wave vectors with respect to time delay. Systematic measurements of $N_{\pm1,\mathbf{k}=\mathbf{0}}(t)$ were performed for each emission component ($\mathrm{I}^{\pm}$) as a function of the increasing incident density power, for various cavity detuning. The results are summarized on Fig. 2, where the peak occupation number $N_{\pm1,\mathbf{k}=\mathbf{0}}(t_{\mathrm{peak}})$, deduced at the luminescence temporal maximum, and taken as representative of the occupancy factor dynamics,[17] has been plotted as a function of the excitation power on logarithmic scales.

Figure 2(b) displays the occupancy dependence on the power density at zero detuning. The component $N_{\pm1,\mathbf{k}=\mathbf{0}}(t_{\mathrm{peak}})$ first increases quadratically with P_{in} in the investigated range under the threshold ($0.3\lesssim P_{\mathrm{in}}\lesssim1$ W cm^{-2}). Then over a narrow power range ($1\lesssim P_{\mathrm{in}}\lesssim3$ W cm^{-2}), it steeply increases, with a rate stronger than quadratic. Finally, for $P_{\mathrm{in}}\gtrsim3$ W cm^{-2}, it grows linearly, reaching values $N_{+1,\mathbf{k}=\mathbf{0}}(t_{\mathrm{peak}})\approx90$ at 7.5 W cm^{-2}. Note that the superquadratic process starts when the peak occupation number $N_{+1,\mathbf{k}=\mathbf{0}}(t_{\mathrm{peak}})$ reaches values comparable to 1. These facts support that, for $\delta=0$, (i) the scattering process is dominated by Coulomb interaction for the major $N_{+1,\mathbf{k}=\mathbf{0}}$ population, and (ii) the process is stimulated by the population in the final state (near $k=0$) of the polariton copolarized with the excitation. In addition, the process is selective with respect to the polariton spin state, since it is not efficient for polariton states of opposite helicity (see, e.g., Refs. 2 and 12).[22] The spin-selective stimulated scattering explains the occurrence of the polarization plateau under pure circular excitation observed in Fig. 1(d).

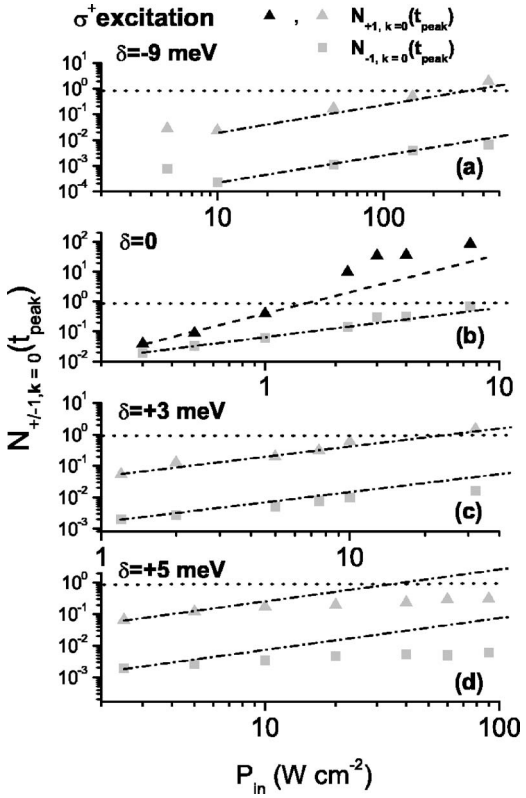

FIG. 2. Circularly polarized excitation σ^+. Occupation factor at temporal peak $N_{\pm1,\mathbf{k}=\mathbf{0}}(t_{\mathrm{peak}})$ corresponding to both emission components $I^{\pm}(t)$ versus incident power density P_{in} for $\delta=$(a)-9, (b) 0, (c) +3, and (d) +5 meV (dashed lines, quadratic increase; dash-dotted lines, linear increase). The horizontal dotted lines indicate an occupation factor equal to 1.

At nonzero detuning, when $|\delta|\gtrsim\Omega_R$, the power dependence of $I^{\pm}$ is much reduced. For the cavity detunings $\delta=-9$ and +3 meV, both occupation factors $N_{+1,\mathbf{k}=\mathbf{0}}(t_{\mathrm{peak}})$ increase linearly with the incident power [Figs. 2(a) and 2(c)], while for $\delta=+5$ meV they increase sublinearly [Fig. 2(d)]. We observe no superquadratic threshold in the emission for any components of luminescence for $\delta\neq0$ [Figs. 2(a), 2(c), and 2(d)], and both $N_{+1,\mathbf{k}=\mathbf{0}}(t_{\mathrm{peak}})$ and $N_{-1,\mathbf{k}=\mathbf{0}}(t_{\mathrm{peak}})$ remain *below* unity in the investigated power range. So the observation of the (super)quadratic process is strongly dependent on the cavity detuning.

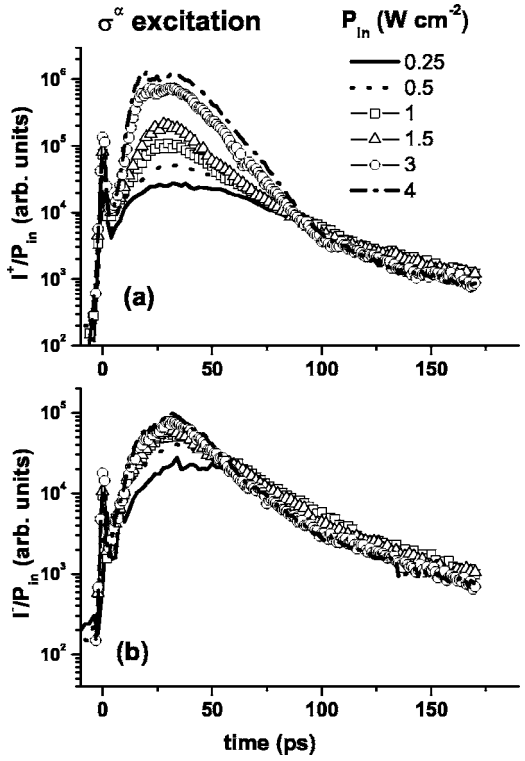

FIG. 3. Elliptically polarized excitation σ^{α} ($\alpha=19°$) Time-resolved emission of the circularly polarized components normalized to the excitation power density $I^{\pm}(t)/P_{\mathrm{in}}$ of the microcavity secondary emission for increasing P_{in}.

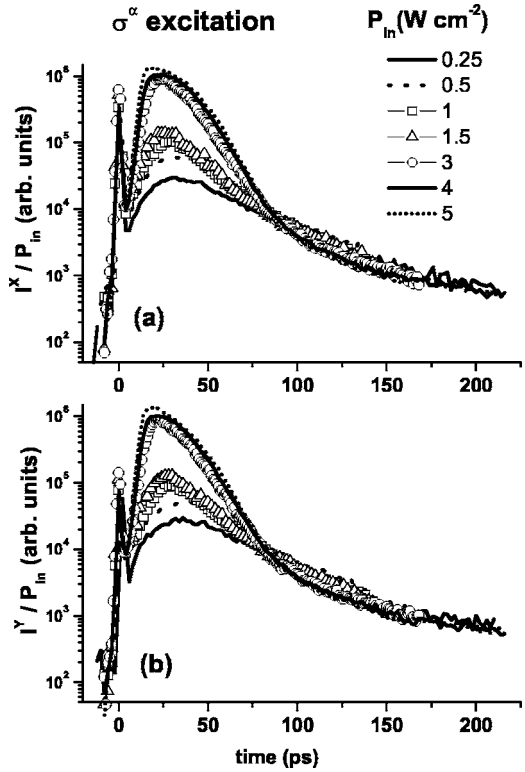

FIG. 4. Elliptically polarized excitation σ^{α} ($\alpha=19°$) Time-resolved emission of the linearly polarized components normalized to the excitation power density $I^{\pm}(t)/P_{\mathrm{in}}$ of the microcavity secondary emission for increasing P_{in}.

We turn now to the experimental description of polariton spin coherence dynamics. In this respect, much can be learnt from the analysis of the secondary emission linear and circular polarization degrees under an elliptically polarized σ^{α} excitation laser beam.[16] We present here the time-resolved microcavity secondary emission for $\delta=0$ after an excitation pulse whose ellipticity is characterized by $\alpha=19°$ (corresponding to $P_{\mathrm{circ},\mathbf{k}_p}=79\%$ and $P_{\mathrm{lin},\mathbf{k}_p}=61\%$). Figure 3 displays the time dependence of the circular polarization components of the LB polariton emission, and Fig. 4 the linear polarization components in the frame (Oxy) defined by the incidence plane, both normalized to the excitation power. When the power density is below the typical value of P_{th} ~ 1 W cm^{-2}, all the polarized components $I^{+(-)}$ and $I^{x(y)}$ increase quadratically.[23] This can be more easily checked on Figs. 5(a) and 5(b), respectively, which represent the incident power dependence of the emission peak occupation numbers $N_{\pm 1,\mathbf{k}=\mathbf{0}}(t_{\mathrm{peak}})$ or $N_{x(y),\mathbf{k}=\mathbf{0}}(t_{\mathrm{peak}})$, deduced using the same calibration procedure as explained above for pure circular excitation.

Above the threshold P_{th}, the behavior of the circular and linear components differs. The I^{+} component increases more than quadratically, for time delays t ranging approximately from 10 to 100 ps [see in particular $N_{+1,\mathbf{k}=\mathbf{0}}(t_{\mathrm{peak}})$ in Fig. 5(a)], while it becomes slightly sublinear for longer time delays [Fig. 3(a)]. In the meantime, the I^{-} component increases less than quadratically [see in particular $N_{-1,\mathbf{k}=\mathbf{0}}(t_{\mathrm{peak}})$ in Fig. 5(a)], but is still superlinear, in the approximate range 10 to 60 ps [Fig. 3(b)]. It becomes sublinear for time delay $t \gtrsim 60$ ps, somewhat earlier than for I^{+}.

By contrast, the linear components $I^{x(y)}$ remain close to each other when P_{in} increases: above the threshold P_{th}, in a very narrow excitation power range ($1 \lesssim P_{\mathrm{in}} \lesssim 3$ W cm^{-2}), and for $10 \lesssim t \lesssim 90$ ps, they increase superquadratically, while they resume a quadratic increase with P_{in} above 3 W cm^{-2} [Figs. 4 and 5(b)]. Finally, at long time delays ($t \gtrsim 90$ ps), they increase sublinearly with P_{in}, like the circular components. Although both linear components have a quite similar dependence on P_{in}, the accurate balance between I^{x} and I^{y} depends in fact on the precise time delay, as we shall see below. We turn now to the examination of the emission polarization degrees.

Figure 6 represents the circular polarization kinetics under elliptical excitation for different excitation powers in the range $0.25 \lesssim P_{\mathrm{in}} \lesssim 4$ W cm^{-2}, as deduced from Fig. 3. At low excitation power, the polariton circular polarization decays with the same characteristic time as under pure circular excitation, the initial value corresponding now to the laser circular polarization degree (79%). However, when $P_{\mathrm{in}} \gtrsim P_{\mathrm{th}}$, the nonsymmetrical behavior of I^{+} and I^{-} is reflected in the circular polarization rate dynamics: before stimulation occurs ($t \lesssim 10$ ps), partial polariton spin relaxation takes place, followed immediately by a transient repolarization, observed for $t \gtrsim 10$ ps. When stimulation increases, the effect becomes so strong that the observed peak of circular polarization becomes *higher* than the excitation laser one, reaching values as high as $P_{\mathrm{circ}}=91\%$ at $P_{\mathrm{in}}=4$ W cm^{-2}. In particular, as the excitation power increases, the effect overcomes the depolar-

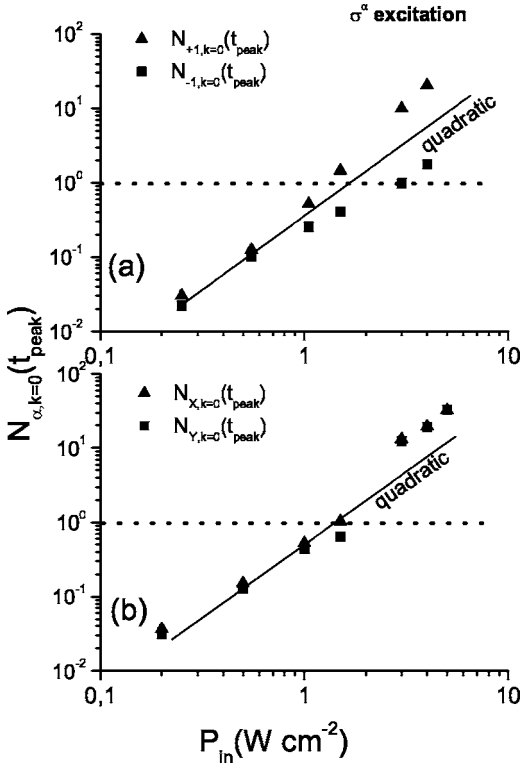

FIG. 5. Elliptically polarized excitation σ^{α} ($\alpha=19°$). (a) The occupancy factors $N_{\pm 1,\mathbf{k}=\mathbf{0}}$; (b) $N_{x(y),\mathbf{k}=\mathbf{0}}$ for increasing excitation power densities ($\delta=0$). Solid line, quadratic increase with P_{in}; dashed line, $N_{\alpha,\mathbf{k}=\mathbf{0}}=1$.

ization process observed in the spontaneous regime.

We turn now to the evaluation of the linear polarization of the generated elliptical polaritons. This allows us to get information on the coherence between $|\mathbf{k}=0,+1\rangle$ and $|\mathbf{k}=0,-1\rangle$ states. Figure 7 displays the dynamics of $P_{\mathrm{lin}}(t)$ for increasing excitation power P_{in} chosen successively in the spontaneous and stimulated regimes. The main general feature is a fast drop occurring just after the excitation pulse, from the initial value $P_{\mathrm{lin}}(t)\approx 61\%$, identical to the linear polarization of the excitation laser,[23] down to much smaller

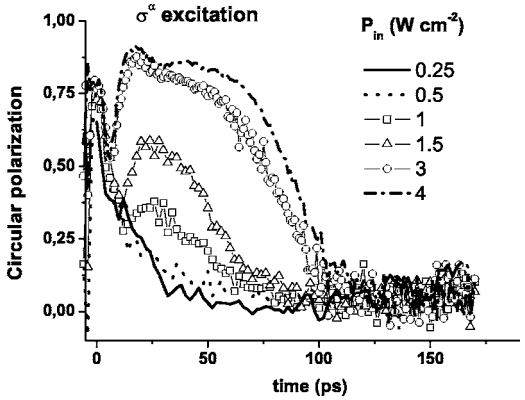

FIG. 6. Elliptically polarized excitation σ^{α} ($\alpha=19°$). Temporal evolution of the resulting circular polarization degree of the polariton emission at $\mathbf{k}=\mathbf{0}$, for increasing excitation power densities ($\delta=0$).

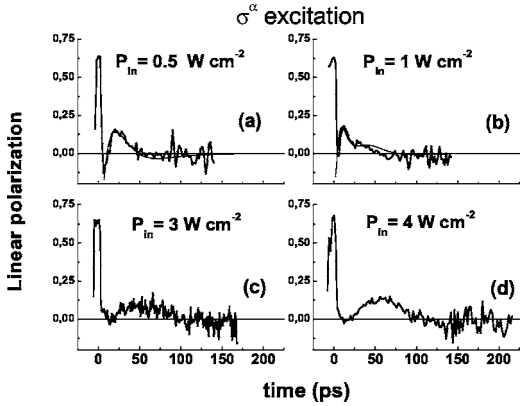

FIG. 7. Elliptically polarized excitation σ^{α} ($\alpha=19°$). Temporal evolution of the resulting linear polarization degree of the polariton emission at $\mathbf{k}=\mathbf{0}$, for increasing excitation power densities ($\delta=0$). Bold lines, experimental data; thin solid lines, fit to the data using a phenomenological pseudospin precession model (see text).

values $|P_{\mathrm{lin}}(t)|\lesssim 0.15$. However, after this fast decay, the linear polarization oscillates, starting from *negative* values when exciting under the threshold P_{th}; this proves that the spin coherence is not completely lost in the scattering processes from $|\mathbf{k}_p,\alpha_p\rangle$ to $|\mathbf{k}=\mathbf{0},\alpha_0\rangle$ states. However, these damped oscillations are nonperiodical, as can be more clearly seen in the linear polarization dynamics at the lowest excitation we could achieve (see Fig. 8). We shall comment on these points in the next section.

Finally, we have performed experiments under pure linearly polarized excitation. It is striking that, after a fast drop, the linear polarization of $k=0$ emitted polaritons deviates from zero, reaching negative values of the order of -10% at low excitation power, as observed on Fig. 8 ($P_{\mathrm{in}}=0.25$ W cm^{-2}). At higher excitation power, both linear polariton emission components are stimulated when P_{in} reaches a threshold comparable to but smaller than P_{th}, as seen on Fig. 9, which shows the emission peak intensities normalized to P_{in}. Both linear components increase more than quadrati-

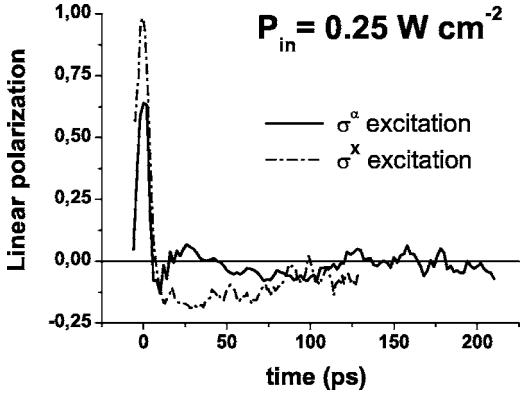

FIG. 8. Temporal evolution of the resulting linear polarization degree of the polariton emission at $\mathbf{k}=\mathbf{0}$, for $P_{\mathrm{in}}=0.25$ W cm^{-2} ($\delta=0$). Solid line, case of elliptically polarized excitation σ^{α} ($\alpha=19°$). The nonperiodical P_{lin} oscillations with time are clearly evidenced. Dash-dotted line, case of linearly polarized excitation σ^{x} ($\alpha=45°$).

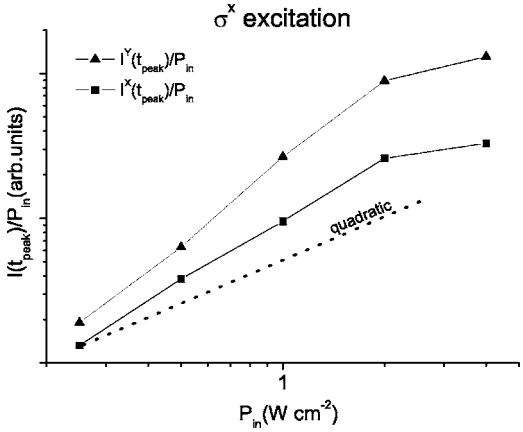

FIG. 9. Linearly polarized excitation σ^x. The incident electric field is in the laser incidence plane. Emission peak intensities of the linear component of the emission normalized to the incidence power density $I^{x(y)}(t_{\text{peak}})/P_{\text{in}}$ for increasing excitation power densities ($\delta=0$). Dashed line, quadratic increase with P_{in}.

cally, and the negative linear polarization increases in absolute value with P_{in}, as the $|\mathbf{k}=\mathbf{0},Y\rangle$ ($\alpha=-\pi/4$) component grows faster than the $|\mathbf{k}=\mathbf{0},X\rangle$ ($\alpha=+\pi/4$) one (Fig. 10). The negative polarization approaches a lower limit of approximately -0.08 for the lowest excitation power $P_{\text{in}}=0.25$ W cm^{-2} as well as for long time delays at higher excitation power when, presumably, the occupation numbers become too small to support stimulated transitions. This suggestion is confirmed by the analysis of the emission intensity as a function of time at large time delays (Fig. 11). Indeed, in the *spontaneous* regime of the bimolecular scattering, when the latter is the dominant population scattering process, the dynamics of the occupation number at the pump wavevector $\mathbf{k}_p$ is approximated by the simple differential equation $dN_{\mathbf{k}_p}/dt=-aN_{\mathbf{k}_p}^2-N_{\mathbf{k}_p}/\tau_{\mathbf{k}_p}$, where a is a bimolecular scattering rate. The approximate solution is $N_{\mathbf{k}_p}(t)=N_{\mathbf{k}_p}(t_0)/[1+N_{\mathbf{k}_p}(t_0)a(t-t_0)]\approx 1/a(t-t_0)$, where the last approximate equality holds at long time delays, and t_0 corresponds to the time when Coulomb scattering evolves from the stimulated

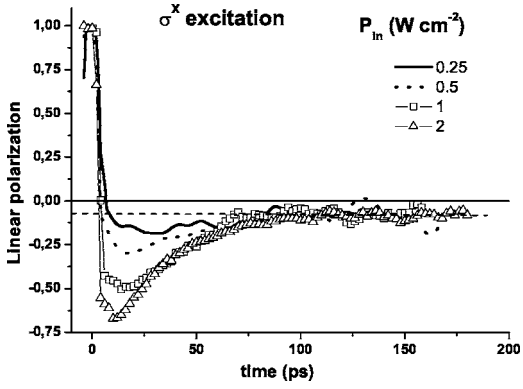

FIG. 10. Linearly polarized excitation σ^x. The incident electric field is in the laser incidence plane. Linear polarization degree of polariton emission for increasing excitation power densities at $\mathbf{k}=\mathbf{0}$ ($\delta=0$). The horizontal dashed line indicates a linear polarization of -0.08 at long time delay.

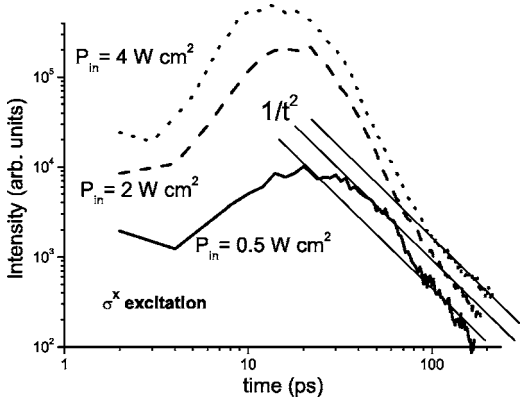

FIG. 11. Linearly polarized excitation σ^x. Emission intensity at $\mathbf{k}=\mathbf{0}$ vs time for $P_{\text{in}}=0.5$ (full line), 2 (dashed line), and 4 W cm^{-2} (dotted line). Straight lines, $1/(t-t_0)^2$ law typical of bimolecular scattering at long time delay.

to the spontaneous regime. The occupation number in $\mathbf{k}=\mathbf{0}$ being given by $dN_0/dt=+(a/2)N_{\mathbf{k}_p}^2-N_0/\tau_0$, and the emission intensity by $I_{\mathbf{k}=\mathbf{0}}\propto N_{\mathbf{k}=\mathbf{0}}/\tau_0$, we finally get ($\tau_0\lesssim t-t_0\lesssim\tau_{\mathbf{k}_p}$) $I_{\mathbf{k}=\mathbf{0}}(t)\propto 1/(t-t_0)^2$. Figure 11 shows the emission intensity as a function of time in double logarithmic scale for different P_{in}. The $1/(t-t_0)^2$ slope is pronounced for all the P_{in} at t exceeding approximately $t_0\approx 80$ ps. Comparing with Fig. 10, one can see that exactly at these time delays the linear polarization is constant within the experimental precision, and equal to -0.08. Thus we attribute this value of polarization to spontaneous polariton-polariton scattering. The origin of the negative linear polarization will be discussed in the next section.

IV. DISCUSSION: POLARITON COHERENT SPIN DYNAMICS AND EXCHANGE INTERACTION

The observed signal in the above time-resolved emission experiments is detected from polaritons around $\mathbf{k}=\mathbf{0}$ escaping from the microcavity, which in turn are produced by scattering from the generated $|\mathbf{k}_p,\alpha_p\rangle$ polariton states. Generally, at low excitation power and $|\delta|\gtrsim\Omega_R$, we can infer from the linearity of the intensity dependence that the scattering process originates from monomolecular processes due to polariton interaction with acoustic phonons, impurities, or even carriers due to residual doping in the barriers.[24,25] On the other hand, for $\delta=0$, we interpret the observed quadratic increase of the intensity ($I^+,I^{x(y)}$) at low excitation power [Figs. 2(b) and 5] as due to polariton mutual Coulomb scattering, from $|\mathbf{k}_p,\alpha_p\rangle\otimes|\mathbf{k}_p,\alpha_p\rangle$ to $|\mathbf{k}_s,\alpha_s\rangle\otimes|\mathbf{k}_i,\alpha_i\rangle$ polariton pair states (the indices s and i stand for signal and idler, respectively). We attribute then the increased efficiency of the bimolecular Coulomb process at zero detuning to the fact that under resonant excitation at $\mathbf{k}_p=10^4$ cm^{-1}, Coulomb single scattering events satisfy the *phase-matching condition*[2,3]

$$2\mathbf{k}_p=\mathbf{k}_s+\mathbf{k}_i, \tag{1}$$

$$E(\mathbf{k}_p) = E(\mathbf{k}_s) + E(\mathbf{k}_i) \tag{2}$$

at zero detuning, but not for $|\delta| \gtrsim \Omega_R$ (here, in our experimental conditions, $\mathbf{k}_s \approx \mathbf{0}$). As a fact, for $\delta=0$, $\mathbf{k}_p$ corresponds here to the LB inflection point. Under these conditions, this also means that for $P_{\text{in}} \gtrsim 0.25\ \text{W cm}^{-2}$, the Coulomb scattering process is already more efficient than the monomolecular scattering processes.

We can further conclude from experiments under pure circular excitation at zero detuning that the Coulomb scattering process conserves the total angular momentum. The major polariton pairs, copolarized with the laser, are scattered by Coulomb interaction to pair states with the same helicity. In terms of polariton angular momentum projection on the Oz quantification axis, we can thus write the additional angular momentum selection rule

$$2J_{z,p} = J_{z,s} + J_{z,i} \quad (J_{z,p} = \pm 1). \tag{3}$$

The polariton population with opposite helicity to the pump, which appears due to partial spin relaxation, remains small. Monomolecular scattering processes are thus more efficient than the Coulomb one for those polaritons [see Fig. 2(b)].

Within the range of wave-vector states populated after a resonant excitation at short time delay (for which $k \ll 1/a_X$, a_X being the bare exciton Bohr radius), exchange terms are expected to be the dominant terms versus the direct one in the Coulomb interaction, as for bare excitons.[26,27] This is confirmed by the experimental fact that, under elliptically or linearly polarized excitation, we have observed the quadratic increase at zero detuning in both co- and cross-polarized components I^x and I^y of the emission (see Sec. III). This property is not allowed by the direct Coulomb term, while it is by the exchange ones.

At higher excitation power, the superquadratic increase in polariton polarized modes $|\mathbf{k},\alpha\rangle$ occurs when the corresponding occupation numbers $N_{\alpha,\mathbf{k}=\mathbf{0}}(t)$ $(\alpha=0,\pi/2,\pm\pi/4)$ become comparable to unity [Figs. 2(b) and 5]. We interpret this as due to stimulated Coulomb scattering between polariton pairs described as quasibosons, in agreement with Refs. 2–7 and 12. The occurrence of the polarization plateau observed in Fig. 1(d) is the manifestation of this process. Note that in our experimental conditions, no stimulated scattering is observed for monomolecular scattering processes, since, due to the short polariton escape time $\tau(\mathbf{k})$ in $\mathbf{k}=\mathbf{0}$, they are not efficient enough to build a coherent polariton population $N_{\alpha,\mathbf{k}=\mathbf{0}}(t)$ comparable to or greater than unity.

To go further in the interpretation, we must invoke a few assumptions about polarized polaritonic systems. First, due to mutual exchange interactions within the LB, the single-polariton states are renormalized, as experimentally observed in Ref. 28 and deduced from the current effective Hamiltonian theory.[4,5] As the exchange interaction k dependence for bare excitons is weak for $k \ll 1/a_X$, this implies a quasirigid shift of the polariton LB with a given angular momentum when the population is dominated, as is the case in our experiments, by the polariton population in $\mathbf{k}_p$ (we estimate at $\delta=0$ that here $10^4 \lesssim N_{\alpha,\mathbf{k}_p}(t) \lesssim 10^5$). Moreover, we infer from the bare exciton case[16] that the polariton renormalization should be spin dependent, leading to the splitting between polariton states with $J_z=+1$ and $J_z=-1$ given by the expression

$$\Omega_{\text{exch}} \approx E_{\text{exch}}(N_{+1,\mathbf{k}_p} - N_{-1,\mathbf{k}_p}) \tag{4}$$

where E_{exch} is a positive constant essentially determined by polariton mutual exchange.[4] The expression (4) implies that no splitting occurs under linear polarization. Under circular excitation, Ω_{exch} can reach values of the order of about 1 meV.[4,5,28]

Moreover, the polariton longitudinal-transverse (LT) splitting $\Omega_{\text{LT}}(\mathbf{k})$,[20,21] already present at low density, should also be taken into account to determine the polariton single-particle states. In the basis $\{|\mathbf{k},+1\rangle,|\mathbf{k},-1\rangle\}$, the single-particle polariton Hamiltonian can be written as

$$\hat{H}(\mathbf{k}) = \frac{\hbar}{2}\begin{pmatrix} \Omega_{\text{exch}} & \Omega_{\text{LT}}(k)e^{-2i\xi_{\mathbf{k}}} \\ \Omega_{\text{LT}}(k)e^{2i\xi_{\mathbf{k}}} & -\Omega_{\text{exch}} \end{pmatrix} \tag{5}$$

where $\xi_{\mathbf{k}}=(Ox,\mathbf{k})$ is the angle of the polariton wave vector and the Ox axis determined by the excitation conditions (see Sec. II). The splitting $\Omega_{\text{LT}}(\mathbf{k})$ is determined by both (i) the optical TE-TM cavity mode splitting and the coupling strength difference of these two modes to exciton modes,[19,20] and (ii) the long-range electron-hole exchange within the exciton at wave vector $\mathbf{k}$.[21] However, at small wave vectors, the LT splitting is mainly determined by the first contribution. Note that $\Omega_{\text{LT}}(0)=0$.

Finally, in order to describe the polarization dynamics, it is more convenient to describe the system evolution in terms of the polariton pseudospin density $\mathbf{S}_{\mathbf{k}}$, defined above in Sec. II. Its time evolution is then given by the coupled set of equations

$$\frac{d\mathbf{S}_{\mathbf{k}}}{dt} = \tilde{\mathbf{\Omega}}_{\mathbf{k}} \times \mathbf{S}_{\mathbf{k}} - \frac{\mathbf{S}_{\mathbf{k}}}{\tau_{\mathbf{k}}} + \left(\frac{d\mathbf{S}_{\mathbf{k}}}{dt}\right)_{\text{Coul}}, \tag{6a}$$

$$\frac{dN_{\mathbf{k}}}{dt} = -\frac{N_{\mathbf{k}}}{\tau_{\mathbf{k}}} + \left(\frac{dN_{\mathbf{k}}}{dt}\right)_{\text{Coul}} \tag{6b}$$

where we have defined $\tilde{\mathbf{\Omega}}_{\mathbf{k}} = \mathbf{\Omega}_{\text{LT}}(\mathbf{k}) + \mathbf{\Omega}_{\text{exch}}$; here, $\mathbf{\Omega}_{\text{exch}} \approx 2(E_{\text{exch}}/\hbar)S_{z,\mathbf{k}_p}\mathbf{e}_z$ represents the exchange effective field, deduced from Eq. (4). The LT splitting is now, in this representation, determined by the fluctuating effective field $\mathbf{\Omega}_{\text{LT}}(\mathbf{k}) = \Omega_{\text{LT}}(k)(\cos\xi_{\mathbf{k}}\mathbf{e}_x + \sin\xi_{\mathbf{k}}\mathbf{e}_y)$, where ξ_{k}, initially set to zero in our pumping geometry, varies at random due to elastic collisions with a typical correlation time τ.

At low excitation intensity, the Coulomb collision as well as renormalization terms in Eqs. (6) are weak, so that the pump pseudospin dynamics $\mathbf{S}_{\mathbf{k}_p}(t)$ is essentially driven by polariton LT splitting $[\tilde{\mathbf{\Omega}}_{\mathbf{k}} \approx \mathbf{\Omega}_{\text{LT}}(k)]$ and time τ.[19] This leads to the exponential decay observed under circular or elliptical excitation, with a characteristic time $T_s^{-1} \sim \langle|\Omega_{\text{LT}}(k_p)|^2\rangle\tau$ typical of the motional narrowing regime (note that the relationship between the spin relaxation time and scattering time is similar to the one of bare excitons[29]). For the presented microcavity, $\Omega_{\text{LT}}(\mathbf{k})$ is estimated to be at most a few tens of μeV[20].

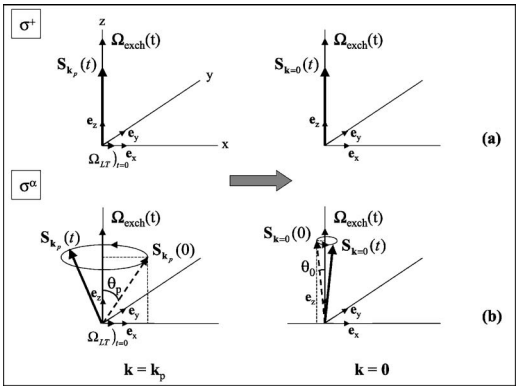

FIG. 12. Sketch of the polariton pseudospin precession at the pump $\mathbf{k}_p$ and detected $\mathbf{k}=\mathbf{0}$ wave vectors in the case of (a) circular excitation σ^+; (b) elliptical excitation σ^α. In the latter case, the spin coherence is partly conserved after the exchange scattering process from $\mathbf{k}_p$ to $\mathbf{k}=\mathbf{0}$ states, but with a sign change. As the pseudospin precesses with the same speed in $\mathbf{k}_p$ and $\mathbf{k}=\mathbf{0}$, coherence can build in $\mathbf{k}=\mathbf{0}$, so linear polarization oscillations can be observed.

When the excitation power is increased, under pure circular excitation, stimulated scattering occurs only on the major spin component $|0,+1\rangle$, leading to the occurrence of the polarization plateau. In addition, at the highest excitation power, the polariton renormalization effect becomes much stronger than the LT splitting so that $\tilde{\mathbf{\Omega}}_{\mathbf{k}}(t)\approx\mathbf{\Omega}_{\mathrm{exch}}(t)$. The initial pseudospin $\mathbf{S}_{\mathbf{k}_p}(0)$ and $\tilde{\mathbf{\Omega}}_{\mathbf{k}}(t)\approx\mathbf{\Omega}_{\mathrm{exch}}(t)$ are thus collinear, both directed along $\mathbf{e}_z$, so that exchange renormalization has a self-stabilizing effect on $\mathbf{S}_{\mathbf{k}_p}(t)$ as long as $\Omega_{\mathrm{exch}}(t)\gg\Omega_{\mathrm{LT}}(\mathrm{k}_p)$, as sketched on Fig. 12(a).

Under elliptical excitation, the initial polariton pseudospin $\mathbf{S}_{\mathbf{k}_p}(0)$ makes an angle $\theta_p=(\mathbf{e}_z,\mathbf{S}_{\mathbf{k}_p})$ with the Oz spin axis, determined by $\theta_p=2\alpha$ (here $\theta_p\approx 38°$). The circular polarization component dynamics can be explained, as in the case of circular excitation, by the fact that stimulated scattering occurs first on the major spin component, which leads to the repolarization of the system near $k=0$ up to the peak value of $P_{\mathrm{circ}}^{\mathrm{max}}$ ($P_{\mathrm{circ}}^{\mathrm{max}}\approx 0.91$ for $P_{\mathrm{in}}=4$ W cm^{-2}). We attribute the subquadratic increase of $N_{-1,\mathbf{k}=\mathbf{0}}(t_{\mathrm{peak}})$ above the threshold to the fact that stimulated scattering of the photogenerated $|\mathbf{k}_p,+1\rangle$ polaritons toward the $|\mathbf{k}=\mathbf{0},+1\rangle$ state becomes then much more efficient than the spin relaxation due to LT splitting in polariton LB. This leads to some $N_{-1,\mathbf{k}_p}$ relative population depletion with respect to the pure spontaneous case in which spin relaxation is still efficient. So, $N_{-1,\mathbf{k}=\mathbf{0}}(t_{\mathrm{peak}})$ hardly reaches unity at the highest investigated excitation power, thus preventing efficient stimulated scattering by occupation of the $|\mathbf{k}=\mathbf{0},-1\rangle$ final state.

The occurrence of linear polarization oscillations with small amplitude is more puzzling. As a fact, the use of the standard bosonic interaction Hamiltonian[16,26] leads, for single scattering events, to equal scattering efficiency from initial pair states $|\mathbf{k}_p,X\rangle\otimes|\mathbf{k}_p,X\rangle$ toward either $|\mathbf{k}=\mathbf{0},X\rangle\otimes|\mathbf{k}=2\mathbf{k}_p,X\rangle$ or $|\mathbf{k}=\mathbf{0},Y\rangle\otimes|\mathbf{k}=2\mathbf{k}_p,Y\rangle$ pairs, and thus to strictly zero linear polarization degree in $\mathbf{k}=\mathbf{0}$. The sign change observed under either elliptical or linear excitation below the threshold (Fig. 8) implies some imbalance between the scattering efficiencies, the creation of a polariton linearly oriented along the Oy axis being slightly more probable than along Ox.

The precise knowledge of the polariton interaction Hamiltonian is a fundamental step in the understanding of the above reported experimental facts. In the polariton strong-coupling region, as said above, exchange terms dominate. The latter can be classified in two types. The terms of the first type, the strongest ones, are responsible for the scattering of polaritons with the same pseudospin; they correspond to the ones determined in Refs. 4, 5, 26, and 27. The second type, corresponding to scattering of polaritons with opposite spin, has been calculated using a second-order perturbation theory.[30] These terms could possibly be at the origin of the specific polarization selection rules in pump-probe experiments under elliptical pump, according to the phenomenological model developed in Ref. 12. The corresponding interaction Hamiltonian in the pseudospin representation would be of the following form, compatible with the axial symmetry of the system:

$$\hat{H}_{SS}=\frac{1}{2}(U-U')\hat{I}+\frac{1}{2}(U+U')\hat{\sigma}_z^1\hat{\sigma}_z^2+U_\perp(\hat{\sigma}_x^1\hat{\sigma}_x^2+\hat{\sigma}_y^1\hat{\sigma}_y^2) \tag{7}$$

where the possible transverse terms of the type $U_\perp(\hat{\sigma}_x^1\hat{\sigma}_x^2+\hat{\sigma}_x^1\hat{\sigma}_x^2)$ are supposed to be negligible.[30] The difference introduced between the coefficients of $\hat{I}$ and $\hat{\sigma}_z^1\hat{\sigma}_z^2$ in $\hat{H}_{SS}$ is equivalent to the introduction of a nonzero interaction term between $|\mathbf{k},+1\rangle\otimes|\mathbf{k}',-1\rangle$ and $|\mathbf{k}+\mathbf{q},+1\rangle\otimes|\mathbf{k}'-\mathbf{q},-1\rangle$ pair states in the usual bosonic Hamiltonians.[31] Such an interaction Hamiltonian $\hat{H}_{SS}$, which still satisfies the total spin conservation, allows in principle the change of polariton alignment in the scattering of a given collinear pair as observed experimentally (using pure linear optical pumping), under the condition that $U'>0$.

Using Eq. (7), one can easily derive the two-particle scattering amplitude. The final state for the Coulomb scattering of two polaritons occupying the same initial state with the ellipticity angle α is, in the Born approximation, given by the following expression:

$$\begin{aligned}
&\hat{H}_{SS}[\cos\alpha|\mathbf{k},+1\rangle+\sin\alpha|\mathbf{k},-1\rangle]_1\otimes[\cos\alpha|\mathbf{k}',+1\rangle\\
&\quad+\sin\alpha|\mathbf{k}',-1\rangle]_2\\
&=[U\cos^2\alpha|\mathbf{k}+\mathbf{q},+1\rangle\\
&\quad+(2U_\perp-U')\sin\alpha\cos\alpha|\mathbf{k}+\mathbf{q},-1\rangle]_1\\
&\quad\otimes|\mathbf{k}'-\mathbf{q},+1\rangle_2+[(2U_\perp-U')\sin\alpha\cos\alpha|\mathbf{k}+\mathbf{q},+1\rangle\\
&\quad+U\cos^2\alpha|\mathbf{k}+\mathbf{q},-1\rangle]_1\otimes|\mathbf{k}'-\mathbf{q},-1\rangle_2.
\end{aligned} \tag{8}$$

In the final state, the phase coherence between the first ("signal") and second ("idler") polaritons is rapidly lost. As a result of this decoherence, the spin state of the "signal" polariton becomes statistical, described by a density matrix. This density matrix, readily obtained by averaging over the spin states of the second polariton, can be written as:

$$A\begin{pmatrix} [U^2+(2U_\perp-U')]+[U^2-(2U_\perp-U')]\cos^2 2\alpha+2U^2\cos 2\alpha & 2U(2U_\perp-U')\sin 2\alpha \\ 2U(2U_\perp-U')\sin 2\alpha & [U^2+(2U_\perp-U')]+[U^2-(2U_\perp-U')]\cos^2 2\alpha-2U^2\cos 2\alpha \end{pmatrix} \tag{9}$$

where A is a dimensionality factor.

Circular and linear polarization of the signal are then found in the usual way from the components of the density matrix:

$$P_{\mathrm{circ},\mathbf{k}=\mathbf{0}}=\frac{2U^2P_{\mathrm{circ},\mathbf{k}=\mathbf{k}_p}}{[U^2+(2U_\perp-U')^2]+[U^2-(2U_\perp-U')^2]P^2_{\mathrm{circ},\mathbf{k}=\mathbf{k}_p}} \approx \frac{2P_{\mathrm{circ},\mathbf{k}=\mathbf{k}_p}}{1+P^2_{\mathrm{circ},\mathbf{k}=\mathbf{k}_p}},$$

$$P_{\mathrm{lin},\mathbf{k}=\mathbf{0}}=\frac{2U(2U_\perp-U')P_{\mathrm{lin},\mathbf{k}=\mathbf{k}_p}}{[U^2+(2U_\perp-U')^2]+[U^2-(2U_\perp-U')^2]P^2_{\mathrm{circ},\mathbf{k}=\mathbf{k}_p}} \approx \frac{2P_{\mathrm{lin},\mathbf{k}=\mathbf{k}_p}}{1+P^2_{\mathrm{circ},\mathbf{k}=\mathbf{k}_p}}\frac{2U_\perp-U'}{U}, \tag{10}$$

where $P_{\mathrm{circ},\mathbf{k}_p}=\cos 2\alpha$ and $P_{\mathrm{lin},\mathbf{k}_p}=\sin 2\alpha$ are the circular and linear polarization degrees of the initial state, respectively. Here approximate equalities correspond to the common case where $|2U_\perp-U'|\ll U$. Similar expressions for P_{circ} and P_{lin} can be obtained for the idler, as it plays a symmetrical part in this approach. However, it is more difficult to observe, due to the efficient scattering processes it undergoes. One can see that, while the circular polarization gives no information on the parameters of interaction, the linear polarization of secondary emission is a direct measure of the ratio $(2U_\perp-U')/U$. We show in the following, on the grounds of microscopic considerations, that in microcavities at negative or zero detuning the linear polarization resulting from the Coulomb scattering of polaritons from around the inflection point should be negative rather than positive. Indeed, the exchange scattering of two polaritons with opposite spins is a second-order process involving "dark" excitons with the angular momentum projection ±2 as intermediate states.[26] Four processes are possible [letters e, h and arrows ↑ (↓) and ⇑ (⇓) are relative to electron and hole and their spin states]:

$$|e_1{\uparrow}h_1{\Downarrow},e_2{\downarrow}h_2{\Uparrow}\rangle \rightarrow |e_1{\downarrow}h_1{\Downarrow},e_2{\uparrow}h_2{\Uparrow}\rangle \rightarrow |e_1{\uparrow}h_1{\Downarrow},e_2{\downarrow}h_2{\Uparrow}\rangle \quad \text{(a)}$$

$$|e_1{\uparrow}h_1{\Downarrow},e_2{\downarrow}h_2{\Uparrow}\rangle \rightarrow |e_1{\uparrow}h_1{\Uparrow},e_2{\downarrow}h_2{\Downarrow}\rangle \rightarrow |e_1{\uparrow}h_1{\Downarrow},e_2{\downarrow}h_2{\Uparrow}\rangle \quad \text{(b)}$$

$$|e_1{\uparrow}h_1{\Downarrow},e_2{\downarrow}h_2{\Uparrow}\rangle \rightarrow |e_1{\downarrow}h_1{\Downarrow},e_2{\uparrow}h_2{\Uparrow}\rangle \rightarrow |e_1{\downarrow}h_1{\Uparrow},e_2{\uparrow}h_2{\Downarrow}\rangle \quad \text{(c)}$$

$$|e_1{\uparrow}h_1{\Downarrow},e_2{\downarrow}h_2{\Uparrow}\rangle \rightarrow |e_1{\uparrow}h_1{\Uparrow},e_2{\downarrow}h_2{\Downarrow}\rangle \rightarrow |e_1{\downarrow}h_1{\Uparrow},e_2{\uparrow}h_2{\Downarrow}\rangle \quad \text{(d)} \tag{11}$$

of which (a) and (b) contribute into scattering without spin flip, and (c) and (d) into spin-flip scattering. The corresponding transition matrix elements are consequently given by the following expressions:

$$-U'=\frac{V_{ee}^2+V_{hh}^2}{E_{\mathrm{LP}}(k)-E_D}, \quad 2U_\perp=\frac{2V_{ee}V_{hh}}{E_{\mathrm{LP}}(k)-E_D} \tag{12}$$

where V_{ee} and V_{hh} are matrix elements of the electron-electron and hole-hole exchange respectively, $E_{\mathrm{LP}}(k)$ is the lower-polariton-energy branch, and E_D is the energy of the dark exciton. Taking into account that, in the vicinity of the inflection point on the lower polariton branch, $E_{\mathrm{LP}}(k)<E_D$, and assuming that $|V_{ee}|\gg|V_{hh}|$,[16,30] one can conclude that $U'\approx V_{ee}^2/[E_D-E_{\mathrm{LP}}(k)]>0$ and $|U_\perp|\ll U'$. Comparing with Eq. (10), we see that $P_{\mathrm{lin},\mathbf{k}=\mathbf{0}}/P_{\mathrm{lin},\mathbf{k}_p}$ should be negative. While inelastic scattering of polaritons by phonons or free carriers may result in *positive* linear polarization of the emission at the signal frequency, *negative* linear polarization is a direct evidence of the two-particle scattering of polaritons with opposite spins. As one can see from Figs. 8 and 10, the polarization is negative for all the values of P_{in}, approaching a lower limit of approximately −0.08 for the lowest $P_{\mathrm{in}}=0.25$ W cm^{-2} as well as for long time delays when the occupation numbers become too small to support stimulated transitions. This behaviour allows us to attribute the value $P_{\mathrm{lin},\mathbf{k}=\mathbf{0}}=-0.08$ to the bimolecular Coulomb scattering of polaritons and to use it for the comparison with the theory. In the case of linearly polarized excitation, under the assumption that $|U_\perp|\ll U'$, $P_{\mathrm{lin},\mathbf{k}=\mathbf{0}}\approx -2U'/U$. Comparing this with the experimental value $P_{\mathrm{lin},\mathbf{k}=\mathbf{0}}=-0.08$, we conclude that for our cavity $U'\approx 0.04U$. The small, as compared to U, positive value of U' is in agreement with the simple microscopic theory given above.

When excitation power increases, stimulation of Coulomb scattering starts, with more efficiency on the dominant final state $|\mathbf{k}=\mathbf{0},Y\rangle$; this increases the negative linear polarization of the observed $\mathbf{k}=\mathbf{0}$ polaritons (Fig. 10). As $U'/U\ll 1$, we expect no significant perturbation on the polariton energy renormalization with respect to expression (4), so that for a linearly oriented polariton ensemble, $\Omega_{\mathrm{exch}}(t)\ll\Omega_{\mathrm{LT}}(k_p)$. The initial pseudospin $\mathbf{S}_{\mathbf{k}_p}(0)$ is then collinear with $\Omega_{\mathrm{LT}}(k_p)$ (along $\mathbf{e}_x$), so that there is no precession motion: the longitudinal-transverse splitting has no effect here on the polariton spin dynamics. As is clear on Figs. 8 and 10, no oscillations of P_{lin} could be observed, and the linear polarization decay at long time delay is slower than in the pure circular case.

Turning back to the elliptical excitation case, we finally describe the polariton pseudospin dynamics in $\mathbf{k}_p$ by the precession of $\mathbf{S}_{\mathbf{k}_p}$ around the self-induced exchange field $\mathbf{\Omega}_{\mathrm{exch}}(t)$ (see Fig. 12). As the polaritons escape from the cavity, the population as well as the pseudospin decay, leading in turn to the decrease of $\Omega_{\mathrm{exch}}(t)$. Finally, this spin precession is observed through scattering to $\mathbf{k}=\mathbf{0}$ states, which inverts and notably reduces in absolute value the linear polarization degree. Note that while the inequality $\Omega_{\mathrm{exch}}(t) \gg \Omega_{\mathrm{LT}}(k_p)$ remains valid, the pseudospin precession occurs practically at the same speed for $\mathbf{k}=\mathrm{k}_p$ and $\mathbf{k}=\mathbf{0}$ states, so that the successive scattering events do not destroy the spin coherence in $\mathbf{k}=\mathbf{0}$. When the population in $\mathbf{k}_p$ vanishes, $\Omega_{\mathrm{exch}}(t)$ decreases, LT splitting becomes dominant, thus leading to the observed final spin relaxation. On Figs. 7(a) and 7(b), for $P_{\mathrm{in}} \lesssim P_{\mathrm{th}}$, we have used a phenomenological law to fit the linear polarization data, according to the function $S_{\mathbf{k}=\mathbf{0},x}(t)=-Ae^{-t/T_s}\cos[\Omega(t)t]$, with $\Omega(t)=\Omega_0 \exp(-t/\tau_p)$. We have here implicitly admitted that the decay of $\Omega(t)$ is mainly governed by some polariton average lifetime τ_p in the LB, which results mainly from the polariton escape from the cavity. T_s represents a characteristic spin decay time. We find $\Omega_0=150\ \mu$eV at $P_{\mathrm{in}}=0.5\ \mathrm{W cm^{-2}}$ and $300\ \mu$eV at $P_{\mathrm{in}}=1\ \mathrm{W\ cm^{-2}}$, taking $T_s=30$ ps and $\tau_p=25$ ps in both cases. Although very rough, this model accounts for the linear polarization evolution at low excitation power. Above the threshold, strong stimulation occurs, so that the beginning of the precession becomes so fast that it cannot be resolved in our experiment (from the previous fit, we infer $\Omega_0 \sim 1$ meV for $P_{\mathrm{in}}=3\ \mathrm{W\ cm^{-2}}$). Then strong pump depletion occurs due to stimulation, and we resume a precession regime with a much lower angular speed, as can be observed experimentally on Figs. 7(c) and 7(d). As the ellipticity is not too strong here, the exchange field still plays a stabilizing role against LT splitting, although less efficient than under circular excitation [it is reduced by the factor $\cos(2\alpha)$ with respect to the latter case].

V. CONCLUSION

In this work, the coherent spin dynamics of microcavity polaritons has been investigated in the Coulomb-scattering-dominated regime. The experiments performed under elliptical excitation conditions support the two major results. (i) The polariton pseudospin evolution is characterized by its precession around the self-induced exchange field which arises due to the imbalance between renormalization terms of differently populated single circular polariton states; the precession movement slows down with time, as polaritons escape from the cavity. (ii) Mutual Coulomb exchange is governed by two kind of terms: the first ones acting on polaritons with the same angular momentum (pseudospin) dominate. They are mainly responsible for the dynamical repolarization observed in the stimulated scattering regime, as well as the renormalization of single-polariton states. The second, much smaller, act on polaritons with opposite angular momenta (pseudospin). In a linearly polarized polariton ensemble, they are responsible for the scattering efficiency imbalance toward pairs with polarization parallel or orthogonal to the initial one, leading to strong negative linear polarization of the signal in the stimulated regime. In an elliptically polarized polariton ensemble they allow us to observe the spin precession of the generated states through the detection of scattered ones. Spin coherence is partly conserved in the scattered states, since in the rigid shift model, the pseudospin of the latter precesses with the same angular speed as the generated ones, but with opposite phase.

The spin structure of the exchange Hamiltonian should also manifest itself in a dense polarized system of bare excitons. However, the specificity of polariton scattering versus exciton scattering makes the interpretation of the experiments easier since (i) the product of the scattering of a polariton pair can be angularly and spectrally resolved due to the strong polariton dispersion at zero or negative detuning; (ii) the $|\mathbf{k},\pm 2\rangle$ dark exciton states do not participate as real, intermediate states in the scattering. They may only play a role as virtual intermediate states in second-order scattering processes, which may be at the origin of the exchange interaction term between polaritons with opposite angular momentum. These specific features should allow us in principle to build a more accurate effective polariton Hamiltonian in terms of an assembly of quasibosons interacting through Coulomb exchange.

ACKNOWLEDGMENTS

We thank M. Combescot, P. Lagoudakis, A. V. Kavokin, and G. Malpuech for fruitful discussions and suggestions. K.K. is grateful to the ACI Polariton project and RFBR for financial support.

[1] C. Weisbuch, M. Nishioka, A. Ishikawa, and Y. Arakawa, Phys. Rev. Lett. **69**, 3314 (1992); R. Houdré, C. Weisbuch, R. P. Stanley, U. Oesterle, P. Pellandini, and M. Ilegems, *ibid.* **73**, 2043 (1994).

[2] P. G. Savvidis, J. J. Baumberg, R. M. Stevenson, M. S. Skolnick, D. M. Whittaker, and J. S. Roberts, Phys. Rev. Lett. **84**, 1547 (2000).

[3] J. J. Baumberg, P. G. Savvidis, R. M. Stevenson, A. I. Tartakovskii, M. S. Skolnick, D. M. Whittaker, and J. S. Roberts, Phys. Rev. B **62**, R16247 (2000).

[4] C. Ciuti, P. Schwendimann, B. Deveaud, and A. Quattropani, Phys. Rev. B **62**, R4825 (2000).

[5] C. Ciuti, P. Schwendimann, and A. Quattropani, Phys. Rev. B **63**, 041303(R) (2001).

[6] M. Saba, B. Deveaud, A. Mura, C. Ciuti, J. L. Staehli, D. Le Si Dang, V. Thierry-Mieg, R. André, S. Kundermann, G. Bongiovanni, and J. Bloch, Nature (London) **414**, 731 (2001).

[7] P. G. Savvidis, C. Ciuti, J. J. Baumberg, D. M. Whittaker, M. S.

Skolnick, and J. S. Roberts, Phys. Rev. B **64**, 075311 (2001).
[8] A. I. Tartakovskii, D. N. Krizhanovskii, and V. D. Kulakovskii, Phys. Rev. B **62**, R13298 (2000).
[9] G. Messin, J. Ph. Karr, A. Baas, G. Khitrova, R. Houdré, R. P. Stanley, U. Oesterle, and E. Giacobino, Phys. Rev. Lett. **87**, 127403 (2001).
[10] S. Hallstein, J. D. Berger, M. Hilpert, H. C. Schneider, W. W. Rühle, F. Jahnke, S. W. Koch, H. M. Gibbs, G. Khitrova, and M. Oestreich, Phys. Rev. B **56**, R7076 (1997); I. A. Shelykh, K. V. Kavokin, A. V. Kavokin, G. Malpuech, P. Bigenwald, H. Deng, G. Weihs, and Y. Yamamoto, *ibid.* **70**, 035320 (2004).
[11] G. Dabasch, T. Baars, M. Bayer, A. Larionov, and A. Forchel, Phys. Rev. B **62**, 13076 (2000).
[12] P. G. Lagoudakis, P. G. Savvidis, J. J. Baumberg, D. M. Whittaker, P. R. Eastham, M. S. Skolnick, and J. S. Roberts, Phys. Rev. B **65**, 161310(R) (2002); A. Kavokin, P. G. Lagoudakis, G. Malpuech, and J. J. Baumberg, *ibid.* **67**, 195321 (2003).
[13] P. Renucci, X. Marie, T. Amand, M. Paillard, P. Senellart, and J. Bloch, in *Proceedings of the 25th International Conference on the Physics of Semiconductors (ICPS), Osaka, (Japan)*, Springer Proceedings in Physics vol. 87, (Springer, Berlin, 2001), Part 1, p. 653.
[14] X. Marie, P. Renucci, S. Dubourg, T. Amand, P. Le Jeune, J. Barrau, J. Bloch, and R. Planel, Phys. Rev. B **59**, R2494 (1999).
[15] M. D. Martin, G. Aichmayr, L. Viña, and R. André, Phys. Rev. Lett. **89**, 077402 (2002).
[16] T. Amand, D. Robart, X. Marie, M. Brousseau, P. Le Jeune, and J. Barrau, Phys. Rev. B **55**, 9880 (1997); P. Le Jeune, X. Marie, T. Amand, F. Romstad, F. Perez, J. Barrau, and M. Brousseau, *ibid.* **58**, 4853 (1998).
[17] P. Renucci, X. Marie, T. Amand, M. Paillard, P. Senellart, and J. Bloch, Phys. Status Solidi A **190**, 407 (2002).
[18] R. M. Stevenson, V. N. Astratov, M. S. Skolnick, D. M. Whittaker, M. Emam-Ismail, A. I. Tartakovskii, P. G. Savvidis, J. J. Baumberg, and J. S. Roberts, Phys. Rev. Lett. **85**, 3680 (2000).
[19] K. V. Kavokin, I. A. Shelykh, A. V. Kavokin, G. Malpuech, and P. Bigenwald, Phys. Rev. Lett. **92**, 017401 (2004).
[20] G. Panzarini, L. C. Andreani, A. Armitage, D. Baxter, M. S. Skolnick, V. N. Astratov, J. S. Roberts, A. V. Kavokin, M. R. Vladimirova, and M. A. Kaliteevski, Phys. Rev. B **59**, 5082 (1999); G. Malpuech (private communication).
[21] E. A. de Andrada e Silva and G. C. La Rocca, Phys. Status Solidi A **190**, 427 (2002).
[22] The observed linear increase of $N_{-1,\mathbf{k}=\mathbf{0}}$ may be attributed to scattering of the $|\mathbf{k}_p,-1\rangle$ polariton population either by acoustical phonons or by carriers present in the well due to nonintentional doping of the cavity. $N_{-1,\mathbf{k}_p}$ arises due to partial spin relaxation of the generated polaritons.
[23] The initial emission peak on a given polarization component is due to Rayleigh scattering due to the surface or interface defects in the Bragg mirrors. See, e.g., W. Langbein and J. M. Hvam, Phys. Rev. Lett. **88**, 047401 (2002). The polarization components of this peak increase *linearly* with the excitation power (see Figs. 3 and 4), and the associated circular and linear polarization degrees are identical to the excitation laser ones.
[24] P. Senellart and J. Bloch, Phys. Rev. Lett. **82**, 1233 (1999).
[25] G. Malpuech, A. Kavokin, A. Di Carlo, and J. J. Baumberg, Phys. Rev. B **65**, 153310 (2002).
[26] C. Ciuti, V. Savona, C. Piermarocchi, A. Quattropani, and P. Schwendimann, Phys. Rev. B **58**, 7926 (1998).
[27] J. Fernandez-Rossier, C. Tejedor, L. Munoz, and L. Viña, Phys. Rev. B **54**, 11582 (1996).
[28] P. G. Savvidis, J. J. Baumberg, R. M. Stevenson, M. S. Skolnick, D. M. Whittaker, and J. S. Roberts, Phys. Rev. B **62**, R13278 (2000).
[29] M. Z. Maialle, E. A. de Andreada e Silva, and L. J. Sham, Phys. Rev. B **47**, 15776 (1993).
[30] Jun-ichi Inoue, Tobias Brandes, and Akira Shimizu, Phys. Rev. B **61**, 2863 (2000).
[31] According to the usual effective exchange Hamiltonian for bare excitons treated as quasibosons, an interaction term exists which couples the optically active ("bright") pair $|\mathbf{k},+1\rangle\otimes|\mathbf{k}',-1\rangle$ to the $|\mathbf{k}+\mathbf{q},+2\rangle\otimes|\mathbf{k}'-\mathbf{q},-2\rangle$ nonoptically active ("dark") ones (Refs. 16 and 26). These "dark" states serve, presumably, as virtual intermediate states for the second-order scattering process responsible for scattering of polaritons with opposite spins (see text). The two-step scattering process to and from dark pair states as the *real* intermediary state was shown to play a major role in the depolarization process of elliptical bright pairs (Ref. 16). However, for $\delta \lesssim \Omega_R$, the probability of this process for polaritons is very small, since it cannot satisfy energy conservation. As a fact, the dark exciton states, denoted $|\mathbf{k},\pm 2\rangle$, are not coupled to cavity optical modes. They lie at the energy $E_D = E_X - \delta_X$ from the bright ones (δ_X is the splitting between bright and dark states due to electron-hole exchange within the exciton, typically of the order of 100 μeV), higher than the polariton modes compared to the thermal energy k_BT, so they are not populated in our experiments. The terms considered in this section are of different nature. Only in the investigated case where $\delta = +5$ meV, are the dark exciton states quasiresonant with the polariton states. Thus, after partial depolarization of circular polaritons, the scattering channel to dark states opens. This may be at the origin of the sublinear increase of $I^{+(-)}$ polarization components under circular excitation observed in Fig. 2(d), the scattering efficiency toward the dark states being quadratic with respect to incident power.